

APPLICATION OF SEMI-GLOBAL HETEROGENEOUS MECHANISMS TO GRAPHITE OXIDATION IN A STAGNATION POINT FLOW

H.K. Chelliah

Department of Mechanical, Aerospace and Nuclear Engineering
University of Virginia
Charlottesville, VA 22903

Keywords: graphite oxidation, heterogeneous mechanisms, simulations

Introduction

Several reacting flow configurations have been used in previous experimental and theoretical studies to investigate the burning rate of graphite and its dependence on external flow fields. One commonly used method involves combustion of graphite particulates in a hot oxidizing environment, typically established by a fuel lean hydrocarbon-air flame.^{1,2} The analysis of gas samples for temperature and species concentration, the particle temperature and size histories have provided quantitative estimates for the surface regression rates and heterogeneous reaction rates. In another experimental method, hot graphite rods placed in a uniform cold oxidizing stream have been used to determine the heterogeneous reaction rates.³ Here the oxidizing stream conditions have been varied to study the effects of flow straining, oxidizer dilutions or enrichments, etc. In theoretical studies,^{1,4-10} semi-global reaction mechanisms have been commonly used to describe the heterogeneous graphite oxidation, while mechanisms ranging from global to detailed have been used for the homogeneous reactions. Although there have been recent efforts to implement elementary mechanisms for heterogeneous reactions, there are many uncertainties associated with the mechanisms and rate data employed.¹¹ Since the available rate data of the semi-global heterogeneous mechanisms can depend on physical properties of the graphite employed in experiments,¹²⁻¹⁴ there is a need to determine the validity of applying these rate data to different graphite shapes, sizes and reacting flow configurations. The objective of the present work is to perform such partial validations of semi-global heterogeneous rates through detailed numerical simulations.

The flow configuration adopted in the present numerical study corresponds to that of the graphite rod oxidation and is discussed below. Based on this flow configuration, comparisons of the burning rate predictions, the gas-phase flame structure and the variation of surface rates as a function of the surface temperature, strain rate, oxidizer concentration and pressure have been performed, but only selected results are presented here for brevity. Efforts are also underway to perform similar simulations of graphite particle oxidation in a quiescent atmosphere.

In addition to the kinetic effects on the graphite burning rate, the gas-phase *CO* flame extinction/ignition phenomena have been examined through numerical calculations. Instead of the experimentally observed extinction/ignition condition, under weak burning conditions the preliminary numerical results indicate a *CO* flame attachment/detachment phenomena.

Flow Configuration

The flow configuration used in the present numerical simulation is similar to that used in Ref. [15] and is shown in Fig. 1. The flow over the graphite rod is assumed to be steady, laminar and two dimensional. If x and y are the coordinates tangential and perpendicular to the graphite surface, respectively, and u and v are the corresponding velocity components, then the outer, inviscid, oxidizer flow can be described by $u_\infty = ax$ and $v_\infty = -ay$, where the subscript ∞ identifies the conditions in the outer flow and a is the velocity gradient in the oxidizer stream. The details of the formulation can be found in Refs. [16-18], the numerical procedure in Ref. [19], the thermodynamic data in Ref. [20], and transport data in Ref. [21]. Introducing the notation $f' = u/u_\infty$, the governing boundary layer equations for mass,

momentum, species and energy in the inner viscous region can be transformed into a system of ordinary differential equations along the stagnation-point stream line ($x=0$) and must be solved subject to the boundary conditions at the surface ($y = y_s$):

$$\begin{aligned} f' &= 0; \quad [\rho Y_i(v + V_i)]_s = \dot{s}_i, \quad i = 1, \dots, N; \\ T &= T_s; \quad (\rho v)_s = \sum_{i=1}^N \dot{s}_i, \end{aligned} \quad (1)$$

and at $y = y_\infty$:

$$f' = 1; \quad Y_i = Y_{i,\infty}, \quad i = 1, \dots, N; \quad T = T_\infty. \quad (2)$$

Here \dot{s}_i is the semi-global mass rate of production or consumption of the i th species by heterogeneous reactions at the surface, ρ is the density in the gas phase, T the temperature, Y_i the mass fraction of the i th species, and V_i the diffusion velocity of the i th species in y direction. In this formulation the burning rate of graphite is equivalent to $(\rho v)_s$. Subscript s identifies the properties at the surface. In the experiments of Makino et al. [3], the temperature of the graphite rod was maintained at a constant value with an external heating source during each burning rate measurement. Since the surface temperature is controlled, heat loss by radiation and heat released at the surface has no effect on T_s , hence the condition $T = T_s$ in Eq. (1) is applicable. However, in simulations of graphite particles in a hot oxidizing environment where such temperature control of the particle surface is absent, heat release by the surface reactions and also heat loss by radiation must be taken into consideration in order to evaluate the surface temperature accurately.¹¹ In all the numerical integrations reported here, the cold oxidizer temperature was set to the experimental condition of $T_\infty = 300$ K.

Reaction Mechanism

The surface reaction pathways have been extensively reviewed by Laurendeau [12] and Essenhigh [13], where it is shown that the overall carbon reactivity can be estimated by $R = \eta A_g \sum_i \dot{s}_i$. In the two heterogeneous reaction mechanisms listed in Tables 1A and 1B (which will be referred to as mechanisms A and B), the terms η (a measure of the species penetration into the solid) and A_g (internal surface area) have been absorbed into the frequency factors A_1 and B_1 .

The rate data of reactions A4 and A5 have been obtained from the experimental burning rate measurements of a graphite rod with a density of $\rho_c = 1.82 \times 10^3$ (kg/m³).³ The rate data of the remaining reactions, i.e. reaction of carbon with OH, O and H₂O in mechanism A are essentially the same as in B. The rate data of mechanism B have been compiled from various sources and are listed in Ref. [1]. Here, the thermal annealing effects have been included in the expression for the reaction $C + (1/2)O_2 \rightarrow CO$, significant only at temperatures above 2000 K. In addition, the data of reaction B5 are for pyrolytic graphite with small particle diameters having negligible internal mass transfer effects.

The gas-phase wet CO reaction mechanism is relatively well known and has been adopted from Yetter et al. [22]. The mechanism consists of 12 species in 28 elementary reactions and is shown in Table 2.

Results and Discussion

Figure 2 shows the predicted burning rate of a graphite rod as a function of surface temperature (T_s) using the two surface reaction mechanisms A and B. The water mass fraction of the oxidizing air stream was set to the experimental value of $Y_{H_2O} = 0.005$. The results with mechanism A are shown for two different strain rates, $a=200$ s⁻¹ and 820 s⁻¹; experimental results of Makino et al. [3] are shown for comparisons. At low temperatures ($T_s < 1200$ K), the reactions A4 ($C_s + CO_2 \rightarrow 2CO$) and A5 ($2C_s + O_2 \rightarrow 2CO$) are insignificant because of their large activation energies. Furthermore, since there is no gas-phase reaction at these temperatures, radicals are almost non-existent so that the remaining reactions are also inactive. As T_s approaches 1300 K, reaction step A5 with an overall activation energy

of 43.0 kcal/mole becomes significant, leading to a rapid increase in the burning rate as seen in Fig. 2. With further increase in T_s , step A4 with relatively higher activation energy (64.3 kcal/mole) becomes important around $T_s \sim 1600$ K and is reflected as a second increment (though mild compared to the first) in the overall burning rate. At $T_s \leq 1200$ K, the surface reactions are slow so that the burning rate is primarily controlled by surface kinetic rates, while at $T_s \geq 2000$ K the surface reactions are very fast and diffusion becomes the rate controlling process. The predictions with mechanism B, however, show significantly lower burning rate for most of the surface temperature range considered. These predictions also fail to show the two-step increase seen with mechanism A.

The differences seen in burning rate predictions between the two mechanisms can be explained based on the relative contributions of the surface reactions to the overall mass burning rate. Figures 3 and 4 show the calculated surface reaction rates using mechanism A and B, respectively, for a uniform air stream at a strain rate $a=200$ s⁻¹. For $T_s \leq 1600$ K, Fig. 3 shows that the dominant surface reaction is A5, while for $T_s \geq 1600$ K the reaction A4 becomes important. The carbon reactions with radical species are always found to be less than the reactions A4 and A5, but its contributions cannot be neglected for the surface temperature range 1400-1700 K. This is not the case with mechanism B. In this case, the reaction B2 ($C + O \rightarrow CO$) is the dominant reaction for $T_s \geq 1400$ K, while surprisingly the reaction B4 is the least important for the whole temperature range considered. In fact the reaction B4 is about two orders of magnitude smaller than A4. The surface reaction rates shown in Fig. 4 are, however, consistent with the results obtained with mechanism B by Bradley and co-workers [1] in their experimental and theoretical investigation on graphite particle oxidation (with mean diameter ≤ 4.3 μm) in a fuel lean methane-air flame (with post flame temperature below 1800 K). According to Ref. [23], the rate data for the reaction B5 strongly depend on the surface temperature and the particle size, and the present comparisons clearly indicate that they are not applicable for burning rate simulations of graphite rods having a diameter of 1 cm and surface temperatures ranging up to 2000 K.

The experiments of Makino et al. [3,5] have shown that two separate critical surface temperatures exist for the CO flame extinction and ignition. However, the numerical calculations employing mechanism A have failed to exhibit such extinction/ignition phenomena for a uniform air stream with a small amount of water vapor ($Y_{H_2O} = 0.005$), and at a strain rate of $a=200$ s⁻¹ and temperature $T_\infty = 300$ K. Instead, a monotonic variation of the CO₂ mass fraction at the flame is observed and is shown in Fig. 5. Because of this smooth attachment/detachment of the flame to the graphite surface when the surface temperature is decreased/increased, the numerical integrations based on steady-state governing equations can proceed from a frozen state to a reacting state. However, when the composition of the oxidizer stream is replaced by oxygen stream (with $Y_{H_2O} = 0.005$) or the pressure of the air stream is increased to 0.79 MPa, the numerical calculations show the existence of a singularity or extinction/ignition phenomena as seen in Fig. 6 at $T_s = 1220$ K. These predicted trends are consistent with the observations made previously by Henriksen [7] in an analytical study employing a weakly burning CO flame regime. However, the flow conditions in the present analysis and that of Henriksen [7] are not exactly the same and more work is needed to verify these observations. On the other hand, if the experimental observations are accurate, then these preliminary results indicate that the semi-global mechanisms are incapable of predicting such extinction/ignition conditions and efforts must be made to include more realistic detailed reaction mechanisms for heterogeneous reactions.

Summary

Numerical simulations of graphite oxidation in a stagnation-point flow field are reported here. The application of semi-global mechanisms determined from previous experiments on oxidation of pyrolytic graphite particles are found to be incapable of predicting the mass burning rates of graphite rods. This clearly indicates the need to accurately characterize the transport effects at the surface and develop elementary reaction mechanisms to describe the graphite oxidation. Furthermore, the results on flame attachment/detachment indicate the need to carefully analyze flow conditions under which flame extinction/ignition will occur and the applicability of the currently available semi-global mechanisms to

such studies.

Acknowledgements

The author would like to thank A. Makino for helpful discussions.

References

- [1] Bradley, D., Dixon-Lewis, G., Habik, S.E., and Mushi, E.M.J., *Twentieth Symposium (International) on Combustion*, The Combustion Institute, p. 931 (1984).
- [2] Mitchell, R.E., *Twenty-second Symposium (International) on Combustion*, The Combustion Institute, p. 69 (1988).
- [3] Makino, A., Araki, N. and Mihara, Y., in preparation.
- [4] Adomeit, G., Hocks, W., and Henriksen, K., *Comb. Flame* **59**, p. 273 (1985).
- [5] Makino, A., and Law, C.K., *Comb. Sci. and Tech.* **73**, p.589 (1990).
- [6] Makino, A., *Comb. Flame* **81**, p. 166 (1990).
- [7] Matsui, K., and Tsuji, H., *Comb. Flame* **70**, p. 79 (1987).
- [8] Henriksen, K., *Twenty-second Symposium (International) on Combustion*, The Combustion Institute, p. 47 (1988).
- [9] Lau, C.W. and Niksa, S., *Comb. and Flame*, **90**, p.45 (1992).
- [10] Makino, A., *Comb. and Flame*, **90**, p.143 (1992).
- [11] Mitchell, R.E., Kee, R.J., Glarborg, P., and Coltrin, M.E., *Twenty-third Symposium (International) on Combustion*, The Combustion Institute, in press (1991).
- [12] Laurendeau, N.M., *Prog. Energy Comb. Sci.* **4**, p. 221 (1978).
- [13] Essenhigh, R.H., "Fundamentals of Coal Combustion," *Chemistry of Coal Utilization*, Second Supplementary Volume, M.A. Elliot (Ed.), Wiley, New York, p. 1153 (1981).
- [14] Howarth, J.B., *Twenty-third Symposium (International) on Combustion*, The Combustion Institute, p. 1107 (1990).
- [15] Chelliah, H.K. and Law, C.K., *ASME - Heat and Mass Transfer in Fires and Combustion Systems*, HTD-Vol 176, p. 49 (1991).
- [16] Smooke, M.D., Puri, I.K., and Seshadri, K., *Twenty-second Symposium (International) on Combustion*, The Combustion Institute, p. 1461 (1988).
- [17] Keyes, D.E. and Smooke, M.D., *J. Comp. Phys.* **73**, p. 267 (1987).
- [18] Miller, J.A., Kee, R.J., Smooke, M.D., and Grcar, J.F., Western States Section of the Combustion Institute, WSS/CI 84-10, April (1984).
- [19] Smooke, M.D., *J. Comp. Phys.* **48**, p.72 (1982).
- [20] Kee, R.J., Miller, J.A., and Jefferson, T.H., "Chemkin: A general purpose, problem-independent, transportable, fortran chemical kinetics code package," Sandia Report, SAND 80-8003.
- [21] Kee, R.J., Warnatz, J., and Miller, J.A., "A fortran computer code package for the evaluation of gas-phase viscosities, conductivities, and diffusion coefficients," Sandia Report, SAND 83-8209.
- [22] Yetter, R.A., Dryer, F.L., and Rabitz, H., *Comb. Sci. and Tech.*, in press (1991).
- [23] Turkdogan, E.T., Koump, V., Vinters, J.V. and Perzak, T.F., *Carbon*, **6**, p. 467 (1968).

Table 1A: Surface-reaction mechanism of Ref. [3], where $\hat{s}_i = \nu_i W_i (\rho Y_i / W_i) A_i T^{\alpha_i} \exp(-E_i / RT)$.

Step	Reaction	A_i	α_i	E_i	Reference
A1	$C_s + OH \rightarrow CO + H$	1.65	0.5	0	[1]
A2	$C_s + O \rightarrow CO$	3.41	0.5	0	[1]
A3	$C_s + H_2O \rightarrow CO + H_2$	6.00×10^7	0.0	64300	[1]
A4	$C_s + CO_2 \rightarrow 2CO$	6.00×10^7	0.0	64300	[3]
A5	$2C_s + O_2 \rightarrow 2CO$	2.00×10^6	0.0	43000	[3]

Note: Units of \hat{s}_i , $A_i T^{\alpha_i}$, E_i , and T are in $\text{kg/m}^2/\text{s}$, m/s , cal/mole , and Kelvin, respectively.

Table 1B: Surface-reaction mechanism of Ref. [1], with the rate \dot{s} expressed in terms of $k_i = B_i T^{\alpha_i} \exp(-E_i/RT)$ and partial pressure P_j .

Step	Reaction	i	B_i	n_i	E_i	\dot{s}_i
B1	$C_s + OH \rightarrow CO + H$	1	6.65×10^2	-0.5	0.0	$\dot{s}_1 = k_1 P_{OH}$
B2	$C_s + O \rightarrow CO$	2	3.61×10^2	-0.5	0.0	$\dot{s}_2 = k_2 P_O$
B3	$C_s + H_2O \rightarrow CO + H_2$	3	9.0×10^3	0.0	68100	$\dot{s}_3 = k_3 P_{H_2O}^{0.5}$
B4	$C_s + CO_2 \rightarrow 2CO$	4	4.8×10^5	0.0	68800	$\dot{s}_4 = k_4 P_{CO_2}^{0.5}$
B5	$C_s + (1/2)O_2 \rightarrow CO$	5	2.4×10^3	0.0	30000	$\dot{s}_5 = \left\{ \frac{k_5 P_{O_2} Y}{1 + k_6 P_{O_2}} \right.$
		6	2.13×10^1	0.0	-4100	$\left. + k_7 P_{O_2} (1 - Y) \right\}$
		7	5.35×10^{-1}	0.0	15200	where
8	1.81×10^7	0.0	97000		$Y = \left[1 + \frac{k_8}{k_7 P_{O_2}} \right]^{-1}$	

Note: Units of \dot{s}_i , E_i , P_j and T are in $\text{kg/m}^2/\text{s}$, cal/mole, atm., and Kelvin, respectively.

Table 2: The specific reaction-rate constants for the $CO/H_2O/O_2$ mechanism from Yetter et al. [22] in the form $k_j = B_j T^{\alpha_j} \exp(-E_j/RT)$.

Step	Reaction	B_j	α_j	E_j
1	$H + O_2 \rightleftharpoons OH + O$	1.91×10^{14}	0.0	16440
2	$H_2 + O \rightleftharpoons OH + H$	5.13×10^4	2.67	6290
3	$H_2 + OH \rightleftharpoons H_2O + H$	2.14×10^8	1.51	3430
4	$OH + OH \rightleftharpoons O + H_2O$	1.23×10^4	2.62	-1878
5	$H_2 + M \rightleftharpoons H + H + M^a$	4.57×10^{19}	-1.4	104380
6	$O + O + M \rightleftharpoons O_2 + M^a$	6.17×10^{15}	-0.5	0
7	$O + H + M \rightleftharpoons OH + M^a$	4.68×10^{18}	-1.0	0
8	$H + OH + M \rightleftharpoons H_2O + M^a$	2.24×10^{22}	-2.0	0
9	$H + O_2 + M \rightleftharpoons HO_2 + M^a$	6.76×10^{19}	-1.42	0
10	$HO_2 + H \rightleftharpoons H_2 + O_2$	6.61×10^{13}	0.0	2130
11	$HO_2 + H \rightleftharpoons OH + OH$	1.70×10^{14}	0.0	870
12	$HO_2 + O \rightleftharpoons OH + O_2$	1.74×10^{13}	0.0	-400
13	$HO_2 + OH \rightleftharpoons H_2O + O_2$	1.45×10^{16}	-1.0	0
14	$HO_2 + HO_2 \rightleftharpoons H_2O_2 + O_2$	3.02×10^{12}	0.0	1390
15	$H_2O_2 + M \rightleftharpoons OH + OH + M^a$	1.20×10^{17}	0.0	45500
16	$H_2O_2 + H \rightleftharpoons H_2O + OH$	1.00×10^{13}	0.0	3590
17	$H_2O_2 + H \rightleftharpoons H_2 + HO_2$	4.79×10^{13}	0.0	7950
18	$H_2O_2 + O \rightleftharpoons OH + HO_2$	9.55×10^6	2.0	3970
19	$H_2O_2 + OH \rightleftharpoons H_2O + HO_2$	7.08×10^{12}	0.0	1430
20	$CO + O + M \rightleftharpoons CO_2 + M^a$	2.51×10^{13}	0.0	-4540
21	$CO + OH \rightleftharpoons CO_2 + H$	1.50×10^7	1.3	-765
22	$CO + O_2 \rightleftharpoons CO_2 + O$	2.51×10^{12}	0.0	47690
23	$CO + HO_2 \rightleftharpoons CO_2 + OH$	6.03×10^{13}	0.0	22950
24	$HCO + M \rightleftharpoons CO + H + M^a$	1.86×10^{17}	-1.0	17000
25	$HCO + H \rightleftharpoons CO + H_2$	7.24×10^{13}	0.0	0
26	$HCO + O \rightleftharpoons CO + OH$	3.02×10^{13}	0.0	0
27	$HCO + OH \rightleftharpoons CO + H_2O$	3.02×10^{13}	0.0	0
28	$HCO + O_2 \rightleftharpoons CO + HO_2$	4.17×10^{13}	0.0	0

Note: Units are cal, mole, cm, and K.

^a The third body efficiencies are $H_2 : 2.5, H_2O : 12.0, CO_2 : 3.8, CO : 1.9$

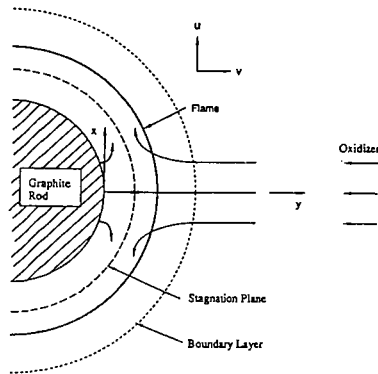


Figure 1: Illustration of the stagnation-point flow field near the graphite rod.

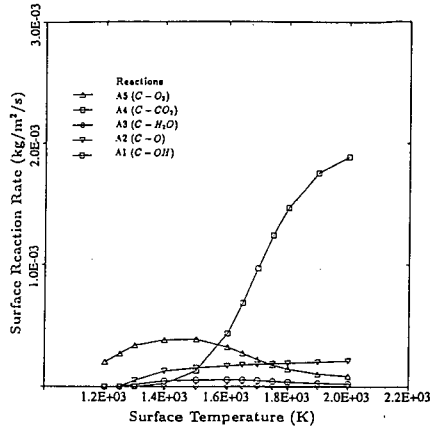


Figure 3: The surface reaction rates of mechanism A as a function of the surface temperature (T_s) in air (with $Y_{H_2O} = 0.005$) at a strain rate of $a=200 \text{ s}^{-1}$.

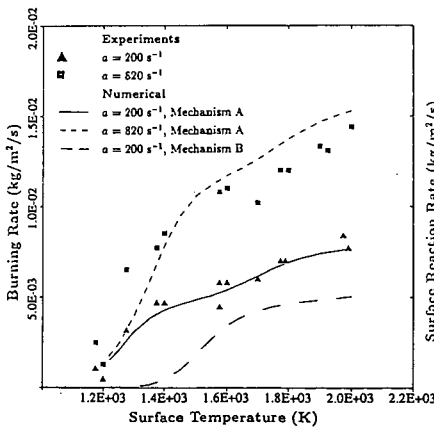


Figure 2: The burning rate of graphite as a function of the surface temperature (T_s) in air (with $Y_{H_2O} = 0.005$) from numerics and experiments of Makino et al. [3], for strain rates $a=200$ and 820 s^{-1} .

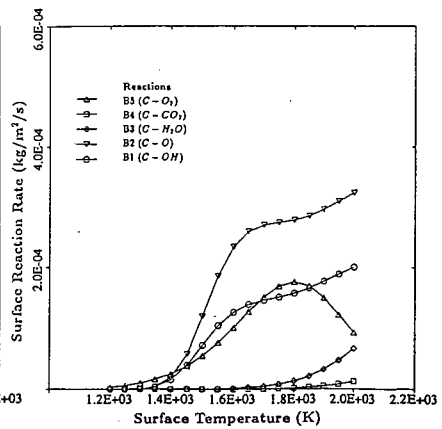


Figure 4: The surface reaction rates of mechanism B as a function of the surface temperature (T_s) in air (with $Y_{H_2O} = 0.005$) at a strain rate of $a=200 \text{ s}^{-1}$.

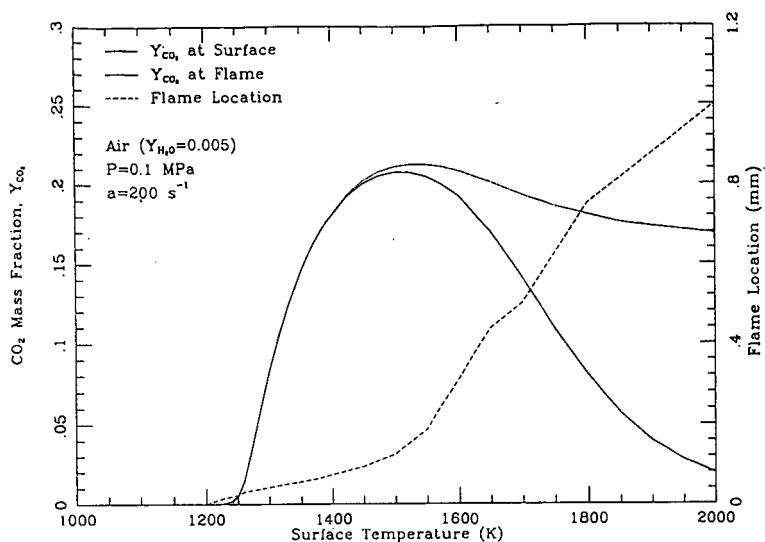


Figure 5: The variation of CO_2 mass fraction at the flame and at the surface, and the flame location as a function of the surface temperature for a air stream at $a = 200 \text{ s}^{-1}$.

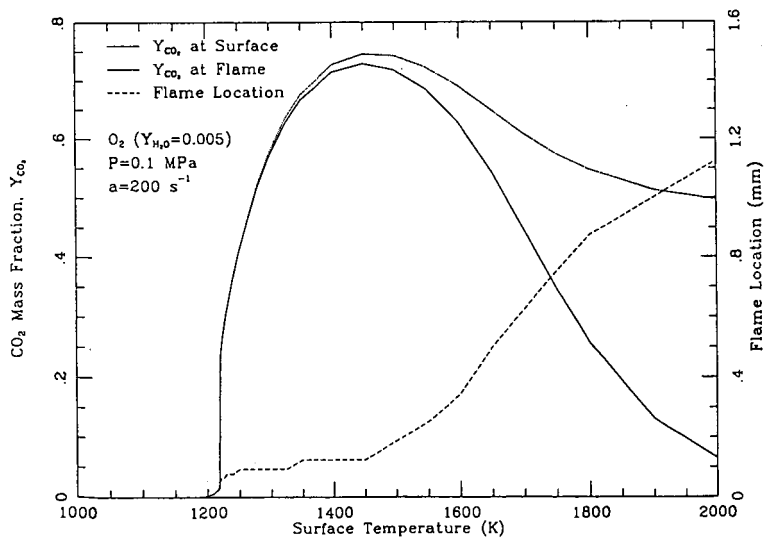


Figure 6: The variation of CO_2 mass fraction at the flame and at the surface, and the flame location as a function of the surface temperature for a oxygen stream at $a = 200 \text{ s}^{-1}$.